Applied and Environmental Microbiology, Sept. 2011, p. 6597–6605 Vol. 77, No. 18
0099-2240/11/$12.00 doi:10.1128/AEM.05588-11

Response of *Pseudomonas putida* KT2440 to Increased NADH and ATP Demand▽†

Birgitta E. Ebert,[1] Felix Kurth,[1] Marcel Grund,[1] Lars M. Blank,[1]* and Andreas Schmid[1,2]

Laboratory of Chemical Biotechnology, TU Dortmund University, Emil-Figge-Str. 66, D-44221 Dortmund, Germany,[1] and Leibniz Institut für Analytische Wissenschaften—ISAS—e.V., Bunsen-Kirchhoff-Str. 11, D-44139 Dortmund, Germany[2]

Received 24 May 2011/Accepted 16 July 2011

Adenosine phosphate and NAD cofactors play a vital role in the operation of cell metabolism, and their levels and ratios are carefully regulated in tight ranges. Perturbations of the consumption of these metabolites might have a great impact on cell metabolism and physiology. Here, we investigated the impact of increased ATP hydrolysis and NADH oxidation rates on the metabolism of *Pseudomonas putida* KT2440 by titration of 2,4-dinitrophenol (DNP) and overproduction of a water-forming NADH oxidase, respectively. Both perturbations resulted in a reduction of the biomass yield and, as a consequence of the uncoupling of catabolic and anabolic activities, in an amplification of the net NADH regeneration rate. However, a stimulation of the specific carbon uptake rate was observed only when *P. putida* was challenged with very high 2,4-dinitrophenol concentrations and was comparatively unaffected by recombinant NADH oxidase activity. This behavior contrasts with the comparably sensitive performance described, for example, for *Escherichia coli* or *Saccharomyces cerevisiae*. The apparent robustness of *P. putida* metabolism indicates that it possesses a certain buffering capacity and a high flexibility to adapt to and counteract different stresses without showing a distinct phenotype. These findings are important, e.g., for the development of whole-cell redox biocatalytic processes that impose equivalent burdens on the cell metabolism: stoichiometric consumption of (reduced) redox cofactors and increased energy expenditures, due to the toxicity of the biocatalytic compounds.

Knowledge of the physiological response of bacteria to environmental stresses and metabolic burdens (e.g., the presence of toxic compounds or recombinant protein overexpression) is of importance in fundamental research to elucidate regulatory mechanisms or basic principles of the metabolic organization and functioning of microbial metabolism. However, a sound understanding of the microbial behavior is equally essential for the development of bioprocesses, as the physiology of the host organisms determines production efficiency (6, 43). Detailed knowledge about the metabolic response and adaptation of microorganisms to specific and often challenging process parameters is key to strain selection. Furthermore, this knowledge allows for the rational engineering of superior production strains and effective process design and control. The interplay of microbial physiology and process performance has long been neglected in bioprocess optimization efforts, which have traditionally focused on biochemical engineering aspects, such as reactor setup and control. However, this issue is becoming increasingly important to establish bio-based processes with high productivity and product yield. These parameters are essential for bio-based processes to be competitive with chemical alternatives not only in the synthesis of high-value pharmaceuticals, but especially for the production of low-value bulk and commodity chemicals, such as biofuels, organic solvents, or plastic monomers (17, 51).

Two stresses that microorganisms are often faced with during biocatalysis are increased energy demand and redox cofactor consumption. This is especially true for oxygenase-based reactions. This enzyme class catalyzes highly interesting reactions, e.g., oxyfunctionalization of nonactivated C-H bonds, with exceedingly high regio-, stereo-, and chemoselectivity that are very difficult to achieve with traditional catalysts (7, 14). Despite their high potential as catalysts, few industrial examples exploiting these enzymes exist (13, 48). The reasons are manifold and can include low enzyme stability, activity, or complex enzyme structure (13). A critical aspect of redox biocatalysis is the need for reduction equivalents, such as NADH. Because of this requirement, oxygenase-based processes are frequently conducted with whole cells instead of isolated enzymes, as metabolically active organisms steadily regenerate the cofactor during catabolism. The imposed increased redox cofactor consumption challenges the metabolism of the host cell. Very high biocatalytic activities might even be limited by the redox cofactor supply if the metabolic redox cofactor regeneration capacity of the microorganisms is approached. Additionally, the biocatalytic substrate and product(s) are often apolar and therefore toxic to the whole-cell biocatalysts, as they intercalate into the cell membrane and perturb its integrity. To separate cells and toxic compounds that are frequently also characterized by a low water solubility, the latter are solved and extracted, in a second organic phase (32, 36). However, solvents with good extraction characteristics for the biocatalytic compounds can be similarly toxic to the cells (10). Microorganisms react to this toxification by different mechanisms, including changes in cell membrane composition,

* Corresponding author. Mailing address: Laboratory of Chemical Biotechnology, Department of Biochemical and Chemical Engineering, TU Dortmund, Emil-Figge-Str. 66, D-44221 Dortmund, Germany. Phone: 49 231 755 7383. Fax: 49 231 755 7382. E-mail: lars.blank@bci.tu-dortmund.de.

† Supplemental material for this article may be found at http://aem.asm.org/.

▽ Published ahead of print on 29 July 2011.

active removal of the toxic substrate by energy-driven efflux pumps, and alteration of the energy metabolism, which significantly increase the cellular energy expenditure. Such demanding conditions might impact the cell physiology and, in consequence, the process performance.

In this work we have investigated and quantitatively describe the physiological response to two metabolic burdens by increased redox cofactor oxidation and ATP hydrolysis activity. We focused on the influence of these perturbations on the redox cofactor regeneration rate and yield as well as mechanisms that might regulate the metabolic activity, as this information is crucial for the design of highly productive redox biocatalysis processes. *P. putida* KT2440 was chosen as a model organism. We consider this species a favorable host for whole-cell redox biocatalysis for the following reasons: *P. putida* strains have proven to have a high NADH regeneration capacity (10) and they are characterized by a low cellular energy demand (28). Low energy expenditure for cell maintenance processes is an advantage for NADH-dependent biocatalysis, as it implies a low consumption of NADH for ATP generation and consequently a high net NADH regeneration rate available for biocatalysis. Furthermore, even at high rates, the carbon breakdown operates without any by-product formation, such as acetate, glycerol, or ethanol, frequently observed with the industrially important hosts *Escherichia coli*, *Bacillus subtilis*, and *Saccharomyces cerevisiae*.

For a whole-cell-based redox biocatalytic process, it is desirable that the host cell reacts to the increased redox cofactor (and energy) demand by adequately raising its metabolic activity to sustain both cellular and biocatalytic demands, thus avoiding deleterious effects on the cell physiology. Indeed, such a "driven-by-demand" control scheme of cellular metabolism was observed with *Escherichia coli* strains: a 1.7-fold increase of the specific glucose uptake rate was achieved by simply increasing the ATP hydrolysis rate (29). In contrast, manifold overexpression of nearly all enzymes of the glycolytic enzymes in yeast did not increase the glycolytic activity (44). Similar to the observation made with *E. coli*, *Pseudomonas* strains challenged with redox biocatalysis react to this metabolic burden by increasing the glycolytic rate but simultaneously decreasing the specific growth rate (10). As redox biocatalysis is intrinsically coupled to both increased ATP and redox cofactor demand, it is not clear which of these two loads triggers the increased metabolic activity. To investigate the effect of these two loads on the metabolism of *P. putida* KT2440 independently, we investigated the response of the organism by addition of 2,4-dinitrophenol (DNP), an uncoupler of oxidative phosphorylation, to the medium and by overexpression of a water-forming NADH oxidase (Nox) gene of *Streptococcus pneumoniae*, respectively. Besides its action as a proton ionophore, DNP gradually inhibits electron transport itself as it is incorporated into the membrane. The manipulation of the ATP synthase activity would be an alternative and a possibly more specific means of altering the ATP consumption rate (29). However, as apolar biocatalytic compounds often intercalate into the membrane, as well, we chose DNP titration to simulate the complex stress imposed by redox biocatalysis.

MATERIALS AND METHODS

Chemicals, bacterial strains, and plasmids. The organisms used in this study were *Pseudomonas putida* KT2440 (5), *Pseudomonas* sp. strain VLB120 (39), *Pseudomonas* sp. strain VLB120ΔC(pHKT1) (23, 40, 47), and *Escherichia coli* DH5α [F^- *endA1 glnV44 thi-1 recA1 relA1 gyrA96 deoR nupG* ϕ80d*lacZ*ΔM15 Δ(*lacZYA-argF*)*U169 hsdR17*(r_K^- m_K^+) λ−] carrying plasmid pYX212 (50). Plasmid pYX212 was kindly provided by Goutham Vemuri (Chalmers University of Technology, Sweden). For the construction of plasmid pCOM10-*nox*, standard cloning procedures were applied (42). Plasmid pYX212 and pCOM10 (45) were isolated from *E. coli* DH5α cultures using the peqGOLD plasmid miniprep kit I (C-Line; Erlangen, Germany). The *S. pneumoniae nox* gene was excised from pYX212 by digestion with BamHI and SalI and purified from a DNA agarose gel using a peqGOLD gel extraction kit (Erlangen, Germany). After digestion of pCOM10 with the same restriction enzymes, dephosphorylation with FastAP thermosensitive alkaline phosphatase (Fermentas, Germany) and purification using the peqGOLD cycle-pure kit (Erlangen, Germany), the *nox* gene and the cut vector were ligated using T4 DNA ligase (Fermentas, Germany). *E. coli* DH5α was transformed with the ligation product via electroporation (EasyjecT; Equibio, Thermo Electron). Successful ligation was checked by the restriction analysis of plasmids isolated from different clones. Transformation of *P. putida* KT2440 with pCOM10-*nox* was done via electroporation.

Media and growth conditions. Lysogeny broth (LB) medium consisting of 5 g $liter^{-1}$ yeast extract, 10 g $liter^{-1}$ tryptone, and 10 g $liter^{-1}$ NaCl was used for standard strain maintenance and solidified, if necessary, through addition of 1.5% (wt/vol) agar. For all other cultivations, M9 mineral medium containing, per liter of deionized water, 8.5 g $Na_2HPO_4 \cdot 2H_2O$, 3.0 g KH_2PO_4, 0.5 g NaCl, 1 g NH_4Cl, 1.2 g $MgSO_4$, and 0.1% (vol/vol) of US* trace element solution (14) was used. The trace element solution consisted of 4.87 g $FeSO_4 \cdot 7H_2O$, 4.12 g $CaCl_2 \cdot 7H_2O$, 1.50 g $MnCl_2 \cdot 4H_2O$, 1.05 g $ZnSO_4$, 0.84 g $Na_2EDTA \cdot 2H_2O$, 0.30 g H_3BO_3, 0.25 g $Na_2MoO_4 \cdot 2H_2O$, 0.15 g $CuCl_2 \cdot 2H_2O$ per liter of 1 M HCl. The pH of all media was adjusted to 7.0. For plasmid selection, kanamycin was added to a concentration of 50 μg ml^{-1}.

2,4-Dinitrophenol titration experiments were performed in 500-ml baffled shake flasks filled with a maximal 50 ml M9 medium complemented with 5 g $liter^{-1}$ glucose. All shake flask cultures were incubated in a rotary shaker at 200 rpm and 30°C. For *nox* overexpression studies, cultivations were performed in 500 ml R′ALF Plus bioreactors (Bioengineering AG, Wald, Switzerland) with a working volume of 250 ml. Process parameters were monitored and controlled at 30°C and a pH of 7.0. Aeration was switched from air to pure oxygen as soon as the pO_2 fell below 20%. For determination of the non-growth-associated ATP demand for cell maintenance, *P. putida* KT2440 was grown at 30°C in continuous cultures at dilution rates of 0.05 to 0.5 h^{-1} using a miniscale chemostat system as developed by Nanchen et al. (34), which allowed for the parallel operation of up to eight 10-ml cultivation vessels. In this setup the feed was provided via a Luer lock needle positioned at mid-liquid level, and mixing was achieved through rising air bubbles. Exhaust gas and culture broth were actively removed by a peristaltic pump through a single tube. The resulting low pressure inside the vessel caused a passive inflow of air at a rate that equaled the pumping rate of the efflux pump. To minimize evaporation, the incoming air was saturated with water by passage through a humidifier. To ensure a constant culture volume, the efflux needle was adjusted at a height marking the 10-ml level. In this way, the volume of culture removed via the efflux equals the medium feed rate. Dissolved oxygen concentrations were not controlled online but were determined in a separate experiment with an airflow rate of 12 ml per min. The dissolved oxygen concentration in the investigated culture of *P. putida* KT2440 growing at a rate of 0.4 h^{-1} was above 50%. Thus, we assumed fully aerobic conditions in all other experiments. All continuous culture experiments were performed with M9 minimal medium containing 1 g $liter^{-1}$ glucose. All physiological parameters were determined during the steady-state phase after at least three volume changes of continuous operation.

Analytical procedures. Cell concentrations were monitored by measuring optical densities with a spectral photometer (Libra S11; Biochrom Ltd., Cambridge, United Kingdom) at a wavelength of 450 nm or 600 nm. Cell dry-weight (CDW) concentrations were inferred from optical densities by a conversion factor determined as described in reference 9.

For the quantification of extracellular metabolites and glucose, samples were taken from the cultures and immediately centrifuged (17,700 × *g* at 4°C for 10 min). The supernatant was analyzed using a LaChrom Elite HPLC system equipped with an L-2130 pump, L-2200 auto sampler (cooled to 4°C), L-2350 column oven, L-2420 UV-VIS detector, and L-2490 refraction index detector (VWR International GmbH, Darmstadt, Germany). For analyte separation, a 308R-Gel.H 300- by 8-mm column with a 048R-Gel.H 40- by 8-mm precolumn

was used (Trentec Analysentechnik, Germany), heated to 40°C, and eluted with 5 mM H_2SO_4 at a flow of 1 ml min^{-1}.

Gas chromatography and mass spectrometry (GC-MS) analysis was carried out using a GC 3800, combined with an MS/MS 1200 unit (Varian Deutschland GmbH, Darmstadt, Germany) for separation of the 15 detectable hydrolyzed proteinogenic amino acids and quantification of the ^{13}C-labeling pattern as described previously (25).

^{13}C-labeling experiments. ^{13}C-tracer experiments were performed in shake flask or bioreactor scale. For shake flask experiments, glucose was used at a starting concentration of 5 g $liter^{-1}$ either as a mixture of 20% (mol/mol) uniformly labeled [U-^{13}C]glucose (Isotec, Miamisburg, OH) and 80% (mol/mol) naturally labeled glucose or 100% [1-^{13}C]glucose (Isotec, Miamisburg, OH). For cultivations in bioreactors, a mixture of 20% (mol/mol) uniformly labeled [U-^{13}C]glucose and 80% (mol/mol) naturally labeled glucose at a total concentration of 10 g $liter^{-1}$ or 20 g $liter^{-1}$ was used. Samples were taken under pseudo-steady-state (exponential growth) conditions and immediately centrifuged (17,700 × *g* at 4°C for 10 min). For the determination of the amino acid labeling patterns, cell pellets were resuspended in 150 μl 6 M HCl and hydrolyzed at 105°C for 6 h or 12 h. The dried hydrolysates were derivatized for GC-MS analysis using 30 μl acetonitrile and 30 μl *N*-(tert-butyldimethylsilyl)-*N*-methyltrifluoroacetamide (Macherey-Nagel GmbH & Co. KG, Germany).

^{13}C-based metabolic flux analysis. FiatFlux (53) was used to calculate metabolic flux ratios and net intracellular flux distributions. The latter calculations were based on the stoichiometric model of *P. putida*'s central carbon metabolism described in reference 10, which was extended with the glyoxylate shunt (see Table S1 in the supplemental material) and constrained with the extracellular flux parameter specific growth rate and specific net carbon uptake rate (calculated from the conversion rate of glucose, gluconate, and 2-ketogluconate) and the determined metabolic flux ratios. Specifically, the following metabolic flux ratios were used: fraction of pyruvate derived through the Entner-Doudoroff pathway (only amenable for [1-^{13}C]glucose-labeled experiments), fraction of oxaloacetate originating from pyruvate, fraction of phosphoenolpyruvate (PEP) originating from oxaloacetate, upper and lower bounds of the fraction of pyruvate originating from malate, and the upper bound of the phosphoenolpyruvate fraction derived through the pentose phosphate pathway. As *P. putida* KT2440 possesses two nicotinamide nucleotide transhydrogenases that interconvert NADH and NADPH, we did not calculate separate NADH and NADPH regeneration rates but give a pooled rate for both cofactors. This net rate of NAD(P)H regeneration was calculated from the determined metabolic fluxes by summation of all rates of NADH- and NADPH-forming reactions minus the NADH and NADPH amount consumed for biomass synthesis.

Enzyme activity assay. NADH oxidase activity was determined during the exponential growth phase. A 10-ml culture volume was taken and immediately centrifuged (4,618 × *g* at −9°C for 15 min), washed with freezing buffer (50 mM potassium phosphate buffer [pH 7], 0.3 mM EDTA), and stored at −20°C. For analysis, the pellet was thawed on ice and resuspended in 3 to 4 ml freezing buffer. Cells were disrupted by triple passage through a French press; the cell debris and membrane were removed by ultracentrifugation (150,000 × *g* at 4°C for 60 min). Total NADH oxidase activity in the soluble fraction was measured spectrophotometrically at 340 nm at 25°C in 50 mM potassium phosphate buffer (pH 7.0), 0.29 mM NADH, and 0.3 mM EDTA (50). One unit of activity was the quantity that catalyzed the oxidation of 1 μmol of NADH per min. Protein was quantified by the Bradford method using bovine serum albumin (BSA) as a standard (12).

Estimation of enzyme competition for NADH. To estimate the competitiveness of the recombinant NADH oxidase with native NADH dehydrogenases of the respiratory chain, we estimated an *in vivo* enzyme activity of the NADH oxidase and the two NADH dehydrogenases, assuming Michaelis-Menten enzyme kinetics. Kinetic parameters of the NADH oxidase were taken from reference 52. As corresponding parameters of the *P. putida* KT2440 NADH dehydrogenases were not available, we used literature values of the corresponding *E. coli* enzymes (16, 31). The competition of these enzymes for NADH was expressed as the ratio of the activity of the NADH oxidase to the total activity of the three considered NADH-dependent enzymes. For comparison to an NADH-dependent biocatalytic reaction, the same calculations were performed with data of the NADH-flavin oxidoreductase StyB, a subunit of the *Pseudomonas* sp. strain VLB120 styrene monooxygenase, by the use of data from reference 37 and M. K. Julsing, D. Kuhn, and B. Bühler (unpublished data). The following data were used: the K_m values for NADH were set to 32 μM, 5 μM, 48 μM, and 21 μM, and the V_{max} values to 1,053 U g_{CDW}^{-1}, 800 U g_{CDW}^{-1}, 2,000 U g_{CDW}^{-1}, and 468 U g_{CDW}^{-1} for the NADH oxidase, the NADH dehydrogenases NDH I and NDH II, and the styrene monooxygenase subunit StyB, respectively.

TABLE 1. Maintenance coefficients obtained with glucose-limited cultures of different *Pseudomonas* strains and *Escherichia coli*

Strain	Maintenance coefficient [mmol $(g_{CDW}/h)^{-1}$][b]	Source or reference
Pseudomonas putida KT2440	0.062 ± 0.003	This study
Pseudomonas sp. strain VLB120	0.037 ± 0.002	This study
Pseudomonas sp. strain VLB120ΔC(pHKT1)[a]	0.021 ± 0.001	This study
Pseudomonas putida S12	0.077	28
Escherichia coli MG1655	0.37 ± 0.09	34

[a] Biofilm isolate of *Pseudomonas* sp. strain VLB120 *styC* knockout mutant carrying the green fluorescent protein-encoding plasmid pHKT1 (23, 40, 47).
[b] The error of the maintenance coefficient is the standard error given by the Microsoft Excel function "linest" used for the least-squares fit.

Estimation of energy demand for cell maintenance. Cells consume the carbon substrate for the synthesis of biomass and for energy generation. The energy is used for the biomass synthesis and for cell maintenance processes, which sustain a viable and active state. This so-called non-growth-associated maintenance energy can be quantified according to Pirt's chemostat model (41):

$$q_{carbon} = \frac{\mu}{Y^{max}} + m_{carbon} \quad (1)$$

where q_{carbon} is the specific rate of carbon source consumption, m_{carbon} the maintenance energy coefficient, and Y^{max} the maximum molar growth yield, i.e., the biomass yield without maintenance-associated processes. The specific growth rate μ equals the dilution rate *D* in a continuous cultivation. The maintenance coefficient, expressed as the carbon source consumption rate required to fulfill the non-growth-associated demand, is determined by extrapolating the least-squares linear fit of the q_{carbon}-*D* pairs to the zero specific growth rate. The least-squares fit was performed using the Microsoft Excel function "linest."

RESULTS

Maintenance metabolism. As the NADH yield per mol carbon source is inversely correlated to the cellular energy demand, i.e., the ATP investment necessary to remain in a viable and metabolically active state, this parameter is of special importance for whole-cell based redox-biocatalysis processes. The energy investment costs are an intrinsic property of an organism, and literature values range from less than 1 mmol $(g_{CDW}/h)^{-1}$ to ca. 20 mmol $(g_{CDW}/h)^{-1}$ (46). In order to determine the energy demand of *P. putida* KT2440, we ran glucose-limited chemostat cultures of this strain at dilution rates between 0.05 h^{-1} and 0.5 h^{-1}. The specific carbon uptake rate increased linearly with the dilution rate, allowing the calculation of cell maintenance requirements according to Pirt's chemostat model (41), as described in Materials and Methods. The determined maintenance energy demand of *P. putida* KT2440 was 0.066 $mmol_{glucose}$ $(g_{CDW}/h)^{-1}$ (Table 1), similar to the value determined for *Pseudomonas putida* S12 (28) and significantly lower than (less than one-fifth of) the requirements of *Escherichia coli* MG1655 (34). Assuming complete glucose oxidation, the glucose demand for non-growth-associated maintenance processes of 0.066 mmol $(g_{CDW}/h)^{-1}$ yields NADH regeneration and ATP formation rates of 0.79 mmol $(g_{CDW}/h)^{-1}$ and 0.92 mmol $(g_{CDW}/h)^{-1}$, respectively. Low energy requirements might be a common feature of *Pseudomonas* strains, as maintenance demands determined for *Pseudomonas* sp. strain VLB120 and a biofilm isolate of its isogenic mutant (Table 1) were even lower than those of *P. putida* KT2440. Furthermore, the energy demand of the biofilm variant of this

TABLE 2. Physiological parameters of *P. putida* KT2440 during growth on glucose and in the presence of different concentrations of the uncoupler 2,4-dinitrophenol

DNP (mg liter^{-1})	Specific growth rate (h^{-1})	Biomass yield (g g^{-1})	Specific carbon uptake rate [mmol (g_{CDW}/h)$^{-1}$]
0	0.73 ± 0.04	0.56 ± 0.04	7.3 ± 0.7
300	0.70 ± 0.04	0.44 ± 0.04	8.9 ± 0.9
500	0.55 ± 0.03	0.33 ± 0.03	9.4 ± 0.9
700	0.43 ± 0.02	0.21 ± 0.02	11.6 ± 1.2
1,100	0.25 ± 0.01	0.19 ± 0.01	7.5 ± 0.8

strain, cultivated under identical growth conditions, was almost half of that observed for its parental strain, indicating that prolonged growth at scarce nutritional conditions, i.e., in a biofilm, can even reduce these requirements long term. These properties qualify the *Pseudomonas* strains for use in energy-limited bioprocesses.

Influence of increased ATP hydrolysis on the *P. putida* metabolism. To simulate energy-demanding bioprocess conditions, we challenged *P. putida* KT2440 by adding DNP to the medium. DNP is a proton ionophore that shuttles protons across the cell membranes. To counterbalance the increased proton influx and to maintain a stable proton motive force over the membrane, the cell has to actively pump out protons by consuming ATP. To increase the ATP hydrolysis rate of *P. putida* KT2440 in a stepwise manner, the organism was cultivated in glucose minimal medium in the presence of DNP concentrations between 300 mg liter^{-1} and 1,100 mg liter^{-1}. Notably, DNP concentrations below 300 mg liter^{-1} did not significantly reduce the specific growth rate and biomass yield (data not shown). Other organisms, e.g., *E. coli* and *Saccharomyces cerevisiae*, react more sensitively to DNP titration and show significantly reduced specific growth rates already at DNP concentrations of 138 mg liter^{-1} (0.75 mM) DNP (11, 21). Interestingly, DNP addition to growing cultures of *E. coli* induced the expression of the glucose dehydrogenase, and growth of this strain in the presence of 184 mg liter^{-1} (1 mM) DNP could be fully restored by addition of pyrroloquinoline quinone (PQQ). The presence of PQQ renders this apo-enzyme fully functional and allows the cell to oxidize glucose in the periplasmic space to gluconate, which is followed by the uptake of this intermediate and intracellular breakdown. This direct oxidative pathway of glucose catabolism is also active in *P. putida* KT2440 and might have contributed to the insensitivity of this strain. The high resistance against DNP stress might also be explained by this organism's ability to alter the fluidity of the cell membrane by adjusting the membrane lipid composition (24) and by the active removal of DNP by solvent efflux pumps whose expression is induced upon the presence of toxic solvents (19).

Above the threshold concentration of 300 mg liter^{-1}, DNP caused a remarkable reduction of the specific growth rate and increase of the specific carbon uptake rate (Table 2). Addition of 700 mg liter^{-1} of this oxidative phosphorylation uncoupler boosted the specific carbon uptake rate to a maximum of ca. 11 mmol (g_{CDW}/h)$^{-1}$ (Table 2), 160% of the specific carbon uptake rate under reference conditions without DNP addition. Simultaneously, specific growth rate and biomass yield decreased to 60% and 30%, respectively. Also at this high level of catabolic activity, no by-products such as acetate could be detected in the fermentation broth. It is possible that the addition of 1,100 mg liter^{-1} of DNP led to toxification of *P. putida*. After a lag phase of 30 h, the strain grew with a maximal specific growth rate of 0.24 h^{-1}, with a biomass yield similar to that observed during the addition of 700 mg liter^{-1} DNP, but with a specific glucose uptake rate that declined to 7.5 mmol (g_{CDW}/h)$^{-1}$.

Next, ^{13}C-labeling experiments were conducted to uncover possible changes in the intracellular flux distribution and to estimate the *in vivo* NADH regeneration rate (see Tables S2A and S3 in the supplemental material). We assumed that due to the presence of nicotinamide nucleotide transhydrogenases in *P. putida* KT2440, NADH and NADPH can easily be interconverted. The calculated NADH regeneration therefore is the total flux of the NADPH and NADH regenerating reactions minus the consumption of these two cofactors for biomass synthesis and cell maintenance.

DNP addition resulted in a considerable increase of the net NADH regeneration rate from 24 to 86 mmol (g_{CDW}/h)$^{-1}$ (Fig. 1A). Apparently, under glucose excess conditions, NADH is regenerated in great abundance (15-fold excess compared to the minimal energy demand determined for glucose-limited growth) and is probably wasted in futile cycles under reference conditions. This excess NADH might allow the cell to be more flexible when reacting to changing growth conditions.

The strong increase of the NADH regeneration rate due to DNP titration was achieved mainly by reducing the carbon flow into biomass and increasing oxidation via the tricarboxylic acid (TCA) cycle (Fig. 2A). Additionally, the data indicated an increased flux through the oxidative pentose phosphate pathway, a pathway that, in pseudomonads, in general, operates exclusively in an anabolic mode to generate biomass precursors. The formation of a partially cyclically operating Entner-Doudoroff pathway and the stark increase of the pyruvate carboxylase flux point to possible metabolic bottlenecks resulting from insufficient pyruvate dehydrogenase activity and enzymatic conversion of glyceraldehyde-3-phosphate to pyruvate.

The high increase of the glycolytic activity and uncoupling from biomass synthesis together with the shift in the metabolic flux distribution resulted in a >6-fold increase of the NADH regeneration rate that could theoretically sustain an NAD(P)H-dependent biotransformation of ca. 1,440 U g_{CDW}^{-1} (assuming that 1 mol NADH is consumed per mol product formed). Reported maximal whole-cell biocatalytic activities of NAD(P)H-dependent enzymes are in the range of 200 to 250 U g_{CDW}^{-1} (20). This difference highlights the potential of *P. putida* KT2440 as a host for redox cofactor-dependent biotransformations. However, the strong increase of the NADH regeneration rate was exposing the strain to energy-demanding conditions, under which NADH is consumed to provide the required ATP and cannot be utilized for redox biocatalysis. For a biocatalytic process, being highly productive, equally high glycolytic activities have to be achieved solely by increasing the NADH demand.

Influence of increased NADH oxidation on the *P. putida* metabolism. To test the metabolic response of *P. putida* KT2440 to an isolated perturbation of the NADH demand, we overexpressed the NADH oxidase of *S. pneumoniae*. This en-

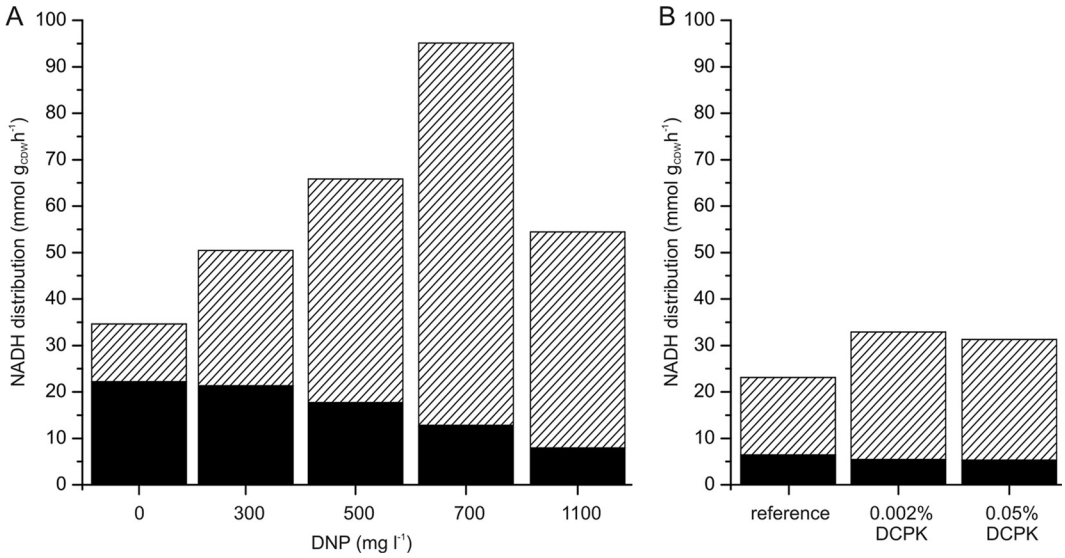

FIG. 1. Distribution of NADH consumption in biosynthetic reactions (black bars) and miscellaneous cellular processes (striped bars) during growth of *P. putida* KT2440 in the presence of different amounts (mg $liter^{-1}$) of DNP (A) and during *nox* overexpression (B). Differences in the NADH consumption rates between the two reference steady states without DNP addition and without NADH oxidase overexpression are due to differences in the exponential growth rate and carbon uptake rate.

zyme is known to be NADH specific and unreactive with NADPH (52). It converts O_2 to H_2O with only a minor formation of hydrogen peroxide (3, 52). Thus, cellular energy demands should not be affected by this enzyme activity, allowing specific investigation of the impact of NADH oxidation on cellular metabolism.

For overexpression of the NADH oxidase gene *nox*, *P. putida* KT2440 was transformed with plasmid pCOM10-*nox*. Expression of *nox* from this plasmid is controlled by the *alk* regulatory system (38), and differential expression was achieved by titration of the inducer dicyclopropylketone (DCPK) to concentrations of 0.002% (vol/vol) and 0.050% (vol/vol), resulting in *in vitro* NADH oxidase activities of 0.07 U $mg_{protein}^{-1}$ and 2.34 U $mg_{protein}^{-1}$. Interestingly, NADH oxidase activity resulted again in an uncoupling of catabolism and anabolism, as visible from the reduction in biomass yield (−26%), but was accompanied by only a modest increase of the glycolytic flux of ca. 7% (Table 3).

^{13}C-based metabolic flux analysis (see Tables S2B and S4 in the supplemental material) revealed only small changes in the flux distribution (Fig. 2B), of which the increase of the TCA cycle flux by ca. 50% was most pronounced. In contrast to the DNP titration experiment, no formation of a cyclic Entner-Doudoroff pathway mode or amplification of the pyruvate shunt could be identified. The estimation of the net NADH regeneration rate from these data showed an increase of the rate from 17 mmol $(g_{CDW}/h)^{-1}$ during reference growth conditions to 27 mmol $(g_{CDW}/h)^{-1}$ when the NADH oxidase was maximally produced (Fig. 1B). Assuming that 45% of the cell dry weight is composed of soluble proteins, the maximal *in vitro* activity of 2.34 U $mg_{protein}^{-1}$ corresponds to an NADH consumption rate of 63 mmol $(g_{CDW}/h)^{-1}$, which is significantly higher than the total NADH regeneration rate estimated under these conditions (Fig. 3). Evidently, the modest increase of the *in vivo* NADH regeneration rate was not sufficient to sustain unlimited activity of the NADH oxidase.

As the actual *in vivo* flux through the NADH oxidase cannot be ascertained, insufficient competition of the enzyme with the native NADH dehydrogenase of the respiratory chain cannot be completely ruled out. The K_m for NADH of the NADH oxidase is 32 μM, and the k_{cat}/K_m of the NADH oxidase is 6.66 s μM^{-1}. *P. putida* KT2440 possesses the two NADH dehydrogenases NDH I and NDH II, encoded by *nuoA* to *-N* and *ndh*, respectively. As no quantitative data for the *P. putida* enzymes were available, we assumed expression and enzyme kinetics similar to those for *E. coli*, for the estimation of competiveness. The enzyme efficiencies are in the same order of magnitude, and thus, all enzymes highly compete for NADH, but no single enzyme outcompetes the others (Fig. 4). Consequently, NADH metabolism of *P. putida* KT2440 should have been significantly perturbed by the presence of NADH oxidase activity. A comparison with the competitiveness of the styrene mono-oxygenase subunit StyB, an NADH-flavin oxidoreductase, corroborates this assumption: though the StyB subunit is considerably less competitive than the Nox oxidase, its activity is sufficient for biocatalytic activity of up to 112 U g_{CDW}^{-1} (4), corresponding to an NADH consumption rate of 7 mmol $(g_{CDW}/h)^{-1}$, ca. 63% of the totally available NADH (4).

DISCUSSION

P. putida KT2440 showed a remarkably metabolic robustness to perturbations of its cellular ATP and NADH demands. DNP at a concentration of 300 mg $liter^{-1}$ almost ceased growth of *E. coli* or *S. cerevisiae* (11, 21) but had little effect on the growth behavior of *P. putida* KT2440. Up to this threshold concentration, growth of the strain was not energy limited, indicating high energy excess under glucose excess growth conditions. At higher DNP concen-

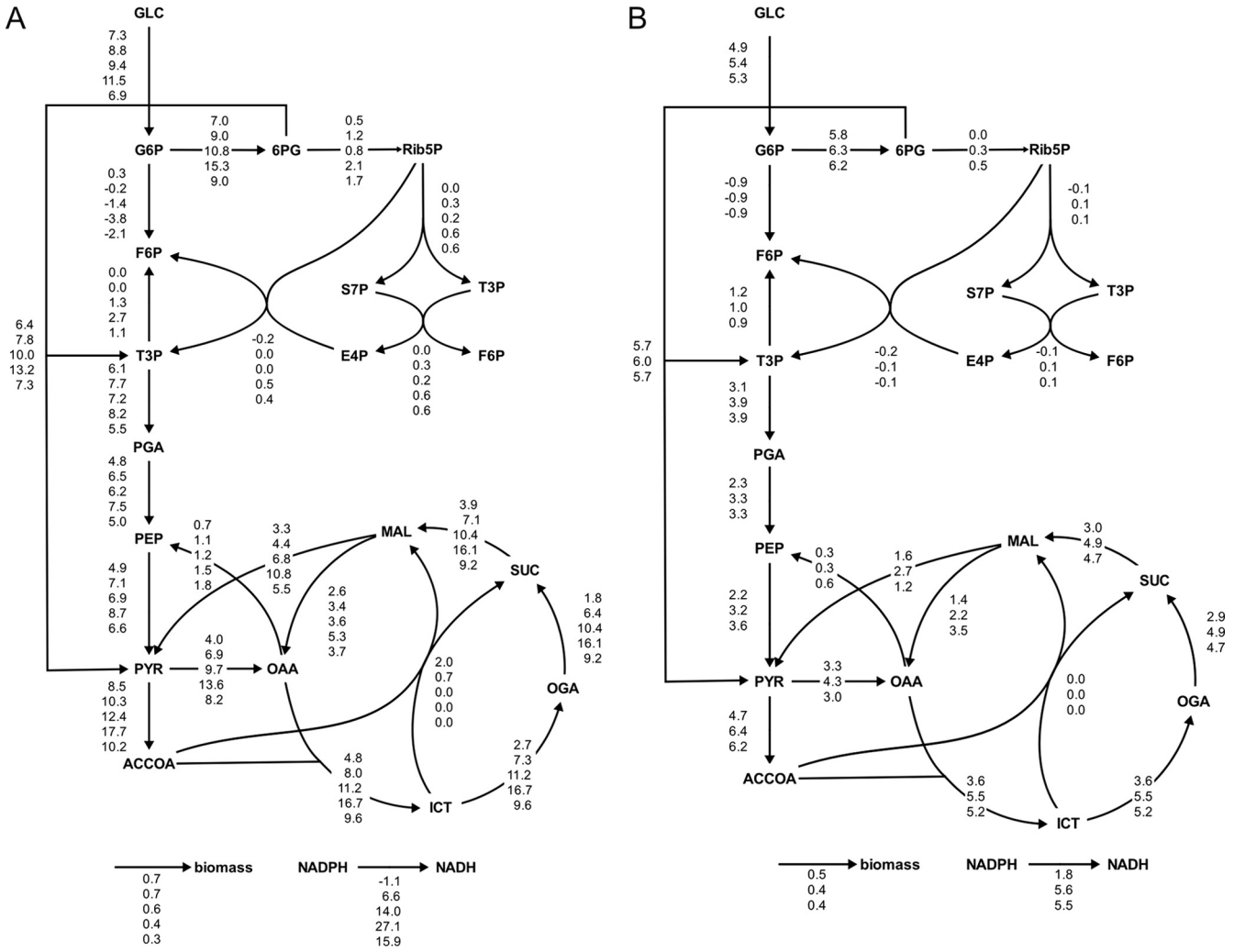

FIG. 2. Metabolic flux distribution of *P. putida* KT2440 grown in the presence of different amounts of DNP (A) and during overexpression of NADH oxidase (B). In panel A, the numbers in each list (from top to bottom) represent reaction rates for growth of *P. putida* KT2440 in the presence of 0, 300, 500, 700, and 1,100 mg liter^{-1} DNP. In panel B, rates in each list (from top to bottom) are given for the reference strain *P. putida* KT2440(pCOM10) and for *P. putida* KT2440(pCOM10-*nox*) induced with 0.002% (vol/vol) and 0.05% (vol/vol) DCPK. On average, the 95% confidence intervals were between 5% and 10% for the major fluxes. Fluxes around the glucose-6-phosphate node and the TCA cycle could be determined only with higher uncertainties. The nonzero fluxes through the glyoxylate shunt in panel A (top values) are a consequence of the very high biomass yields determined for the reference state and the culture containing 300 mg liter^{-1} DNP. If this pathway was excluded, the carbon balance did not close. Abbreviations: GLC, glucose; G6P, glucose-6-phosphate; F6P, fructose-6-phosphate; E4P, erythrose-4-phosphate; S7P, seduheptulose-7-phosphate; T3P, triose-3-phosphate; PGA, 3-phosphoglycerate; OGA, 2-oxoglutarate; PYR, pyruvate; MAL, malate; OAA, oxaloacetate; PEP, phosphoenolpyruvate; ACCOA, acetyl coenzyme A; ICT, isocitrate; 6PG, 6-phosphogluconate; Rib5P, ribose-5-phosphate.

trations, growth was significantly energy limited. Under these conditions, an almost doubled specific carbon uptake rate enabled less than 50% of the specific growth rate observed under reference growth conditions.

Increased glycolytic activities as a response to an imposed metabolic burden have been observed for *E. coli* and *Lactococcus lactis*, in which ATP hydrolysis was modulated by overproduction of the soluble part of the F_1 domain of the F_1F_0-

TABLE 3. Physiological parameters of recombinant *P. putida* KT2440 strains during growth on glucose and with different NADH oxidase levels[a]

Plasmid	DCPK (% [vol/vol])	Specific growth rate (h^{-1})	Biomass yield (g g^{-1})	Specific carbon uptake rate [mmol (g_{CDW} h)$^{-1}$]	*In vitro* Nox activity (U $mg_{protein}^{-1}$)
pCOM10	0	0.48 ± 0.02	0.53 ± 0.02	5.1 ± 0.2	0.01 ± 0.00
pCOM10-*nox*	0.002	0.43 ± 0.03	0.43 ± 0.02	5.6 ± 0.5	0.09 ± 0.03
pCOM10-*nox*	0.05	0.39 ± 0.02	0.39 ± 0.02	5.5 ± 0.5	2.34 ± 0.22

[a] The values of specific growth rate, biomass yield, and specific carbon uptake rate were calculated during the exponential phase of growth, identified by the linear region in the ln(CDW)-versus-time plot.

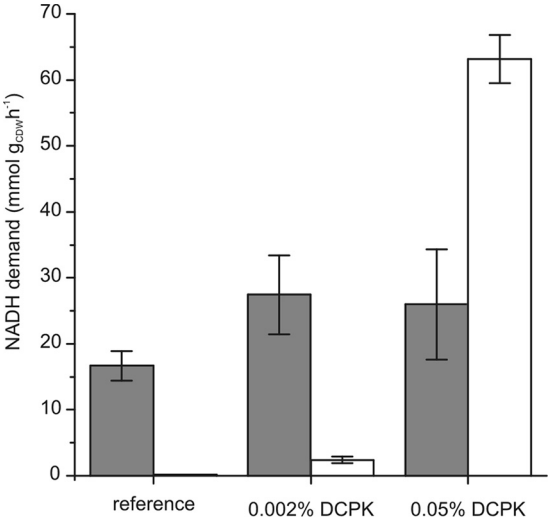

FIG. 3. *In vivo* net NADH regeneration rate (black bars) versus *in vitro* NADH oxidase activity (white bars). The *in vitro* enzyme activity (U $mg_{soluble\ protein}^{-1}$) was translated into an NADH consumption rate [mmol $(g_{CDW}\ h)^{-1}$], assuming that the soluble protein fraction constitutes 45% of the cell dry weight.

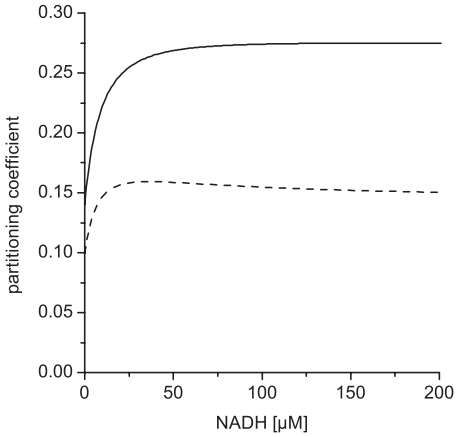

FIG. 4. Competitiveness of NADH oxidase (solid line) and NADH-flavin oxidoreductase StyB (dashed line), a subunit of the *Pseudomonas* sp. strain VLB120 styrene monooxygenase, to native NADH-dependent enzymes. The partitioning coefficient is defined as the fraction of NADH oxidized by the NADH oxidase or oxidoreductase to the total NADH consumption. As the sum of NADH-dependent enzyme activities, estimated values for the NADH dehydrogenases NDH I and NDH II and the Nox or StyB activity were taken. See Materials and Methods for details.

H^+-ATPase (29, 30). The recombinant *E. coli* increased the glycolytic flux to 170% of the wild-type strain and showed a decline in growth rate by 24%. *L. lactis* cells growing in batch culture responded to the increased ATP consumption by growth rate reduction to 69% of that of the reference strain but showed no increase of the glycolytic activity. Resting cells of this strain increased the specific glucose uptake rate to the rate observed with unlimited growing cells (2.7-fold increase), indicating that the extent to which ATP demand controls glycolytic activity depends on the excess capacity of this pathway.

The sensitivity of the metabolic activity to changes in the ATP consumption rate has been explained by the requirement of a high and homeostatic adenylate energy charge (AEC) ([ATP] + 0.5 ADP)/([ATP] + [ADP] + [AMP]) as a driving force for biosynthetic reactions (1, 2). To maintain this thermodynamic nonequilibrium state under various growth conditions that influence both energy supply and consumption, ATP generation and consumption have to be carefully regulated. To achieve this homeostasis, highly sensitive thermodynamic buffering systems have evolved to equilibrate ATP supply and demand, e.g., via regulated uncoupling, storage polymer synthesis/degradation (polyhydroxyalkanoates [PHA] and polyphosphate), futile cycles, or metabolic activation/inhibition of central carbon enzymes in dependence on the energy charge (27).

Of similar importance for the metabolic activity is the redox state of the cell. A steady flux through $NAD(P)^+$-dependent dehydrogenases of central carbon metabolism pathways requires efficient reoxidation of the reduced nucleotides. Accordingly, the activities of several enzymes are known to depend on the NADH level or the NADH/NAD^+ ratio (15, 18, 22, 33). The secretion of reduced by-products by *E. coli* and *S. cerevisiae*, above a certain threshold value of the specific glucose uptake rate, is reported to be due to high NADH/NAD^+ ratios and is a means to reduce the NADH yield and to enhance the NAD^+ regeneration rate. Under such growth conditions, overexpression of an NADH oxidase in *E. coli* (49) increased both the specific growth rate (+20%) and specific glucose uptake rate (+100%), while acetate secretion was halved. Because of presumably derepressed and increased TCA cycle activity and associated increased CO_2 formation, the biomass yield declined to 60% of that of the reference strain. In the same study, *nox* overexpression was investigated with an isogenic *E. coli* strain deficient in ArcA. ArcA is a two-component signaling system of *E. coli*, reported to repress TCA cycle and respiration activities dependent on the redox state. In the ArcA mutant, *nox* overexpression resulted in a complete cessation of acetate formation and was accompanied by an increase in the specific growth rate and protein production. Glucose consumption, however, was not affected by this additional perturbation and remained at around 13 mmol $(g_{CDW}/h)^{-1}$, indicating a possible upper bound of the glycolytic capacity of *E. coli*. Similarly, *nox* overexpression in *S. cerevisiae* decreased the formation of glycerol (26); a sink for electrons from NADH in the cytosol (8), however, did not result in elevated glycolytic activity of this organism. The specific growth rate was also not affected. Evidently, the NADH/NAD^+ ratio has high control of the metabolism of these species.

In contrast to these observations, but in line with our study, considerable NADH oxidase overexpression did not result in a profound acceleration of the glycolytic flux in *L. lactis* (35). As both organisms, *P. putida* and *L. lactis*, did not operate the metabolism at maximal speed, these results indicate that the NADH demand does not exert substantial control of the glycolytic activity in these strains. Rather, increased ATP hydrolysis and possible changes in the energy charge might stimulate elevated glucose catabolism. It is likely that the NADH dehydrogenases compete with the NADH oxidase for NADH to an extent sufficient to satisfy the cellular ATP demand. Furthermore, *P. putida* can partially uncouple ATP generation

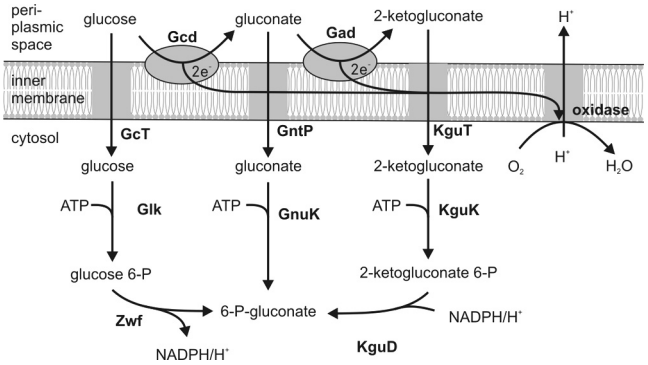

FIG. 5. Glucose uptake pathways of *P. putida* KT2440. Glucose is either directly taken up via the transporter GcT, phosphorylated to glucose-6-phosphate, and oxidized to 6-P-gluconate via glucokinase Glk and glucose-6-phosphate dehydrogenase Zwf or oxidized in the periplasm to gluconate and further to 2-ketogluconate via the glucose dehydrogenase Gcd and gluconate dehydrogenase Gad. Gluconate and 2-ketogluconate are converted in the cytoplasm to 6-phosphogluconate via gluconokinase GnuK or via 2-ketogluconate kinase KguK and 2-ketogluconate 6-phosphate reductase KguD, respectively. The alternative pathways differ in the net formation of reducing equivalent NAD(P)H, as the electrons freed by the membrane-bound dehydrogenases Gcd and Gad are directly transferred to the enzymes of the respiratory chain. P, phosphate.

from NADH formation by redirecting glucose degradation from the phosphorylative to the direct oxidative pathway via glucose dehydrogenase and gluconate dehydrogenase. These enzymes oxidize glucose to gluconate and 2-ketogluconate in the periplasm, while reducing the respiratory chain component PQQ and bypassing the NADPH-generating glucose-6-phosphate dehydrogenase.

By glucose oxidation via the phosphorylative pathway (Fig. 5), two electrons are released in each oxidation step from glucose to gluconate and 2-ketogluconate and used to reduce PQQ. PQQ is reoxidized by passing the electrons to ubiquinone in the membrane. Further electron transport steps via different oxidases to the final electron acceptor oxygen are coupled to proton transfer over the membrane. The generated proton gradient is used to drive ATP generation via the ATP synthase. Both gluconate and 2-ketogluconate can be taken up and catabolized to 6-phosphogluconate, which in the case of 2-ketogluconate uptake costs one NADPH. In fact, the induction of NADH oxidase expression was accompanied by an increase of extracellular gluconate and 2-ketogluconate, indicating an increased flux through this pathway.

In summary, the high resistance against energetic stresses, low maintenance demands, and the ability to catabolize glucose at high rates, without by-product formation, characterize *P. putida* KT2440 as a suitable host for whole-cell bioprocesses. However, when aiming to establish highly productive redox biocatalytic processes with this strain, one has to face high competition for the vital redox cofactor and sophisticated metabolic mechanisms to counterbalance the imposed perturbation of the NADH metabolism. For the design of a superior redox biocatalysis host, metabolic engineering strategies that tightly couple glucose oxidation to NADH reduction have to be developed.

ACKNOWLEDGMENTS

We thank Goutham Vemuri for providing plasmid pYX212, Rainer Gross for the biofilm isolate of *Pseudomonas* sp. strain VLB120ΔC (pHKT1), and Jonathan Collins for proofreading the manuscript. We are grateful to the reviewers for their critical comments and valuable suggestions.

We acknowledge financial support by the German Ministry of Science and Education (BMBF, Project ERA-NET SysMO, no. 0313980A) (VAPMdS) and by the Ministry of Innovation, Science, Research and Technology of North Rhine-Westphalia (Bio.NRW, Technology Platform Biocatalysis, RedoxCell).

REFERENCES

1. **Andersen, K. B., and K. V. Meyenburg.** 1977. Charges of nicotinamide adenine nucleotides and adenylate energy charge as regulatory parameters of metabolism in *Escherichia coli*. J. Biol. Chem. **252:**4151–4156.
2. **Atkinson, D. E.** 1968. Energy charge of the adenylate pool as a regulatory parameter. Interaction with feedback modifiers. Biochemistry **7:**4030–4034.
3. **Auzat, I., et al.** 1999. The NADH oxidase of *Streptococcus pneumoniae*: its involvement in competence and virulence. Mol. Microbiol. **34:**1018–1028.
4. **Bae, J. W., et al.** 2010. Development of a recombinant *Escherichia coli*-based biocatalyst to enable high styrene epoxidation activity with high product yield on energy source. Process Biochem. **45:**147–152.
5. **Bagdasarian, M., et al.** 1981. Specific-purpose plasmid cloning vectors. II. Broad host range, high copy number, RSF1010-derived vectors, and a host-vector system for gene cloning in *Pseudomonas.* Gene **16:**237–247.
6. **Bertau, M.** 2002. How cell physiology affects enantioselectivity of the biotransformation of ethyl 4-chloro-acetoacetate with *Saccharomyces cerevisiae*. Biocatal. Biotransformation **20:**363–367.
7. **Besse, P., and H. Veschambre.** 1994. Chemical and biological synthesis of chiral epoxides. Tetrahedron **50:**8885–8927.
8. **Bjorkqvist, S., R. Ansell, L. Adler, and G. Liden.** 1997. Physiological response to anaerobicity of glycerol-3-phosphate dehydrogenase mutants of *Saccharomyces cerevisiae*. Appl. Environ. Microbiol. **63:**128–132.
9. **Blank, L. M., B. E. Ebert, B. Bühler, and A. Schmid.** 2008. Metabolic capacity estimation of *Escherichia coli* as platform for redox biocatalysis: constraint based modeling and experimental verification. Biotechnol. Bioeng. **100:**1050–1065.
10. **Blank, L. M., G. Ionidis, B. E. Ebert, B. Buhler, and A. Schmid.** 2008. Metabolic response of *Pseudomonas putida* during redox biocatalysis in the presence of a second octanol phase. FEBS J. **275:**5173–5190.
11. **Blank, L. M., and U. Sauer.** 2004. TCA cycle activity in *Saccharomyces cerevisiae* is a function of the environmentally determined specific growth and glucose uptake rates. Microbiology **150:**1085–1093.
12. **Bradford, M. M.** 1976. A rapid and sensitive method for the quantitation of microgram quantities of protein utilizing the principle of protein-dye binding. Anal. Biochem. **72:**248–254.
13. **Bühler, B., and A. Schmid.** 2004. Process implementation aspects for biocatalytic hydrocarbon oxyfunctionalization. J. Biotechnol. **113:**183–210.
14. **Bühler, B., B. Witholt, B. Hauer, and A. Schmid.** 2002. Characterization and application of xylene monooxygenase for multistep biocatalysis. Appl. Environ. Microbiol. **68:**560–568.
15. **Causey, T. B., K. T. Shanmugam, L. P. Yomano, and L. O. Ingram.** 2004. Engineering *Escherichia coli* for efficient conversion of glucose to pyruvate. Proc. Natl. Acad. Sci. U. S. A. **101:**2235–2240.
16. **Chang, A., M. Scheer, A. Grote, I. Schomburg, and D. Schomburg.** 2009. BRENDA, AMENDA and FRENDA the enzyme information system: new content and tools in 2009. Nucleic Acids Res. **37:**D588–D592.
17. **Christensen, C. H., J. Rass-Hansen, C. C. Marsden, E. Taarning, and K. Egeblad.** 2008. The renewable chemicals industry. ChemSusChem **1:**283–289.
18. **de Graef, M. R., S. Alexeeva, J. L. Snoep, and M. J. T. de Mattos.** 1999. The steady-state internal redox state (NADH/NAD) reflects the external redox state and is correlated with catabolic adaptation in *Escherichia coli*. J. Bacteriol. **181:**2351–2357.
19. **Dominguez-Cuevas, P., J. E. Gonzalez-Pastor, S. Marques, J. L. Ramos, and V. de Lorenzo.** 2006. Transcriptional tradeoff between metabolic and stress-response programs in *Pseudomonas putida* KT2440 cells exposed to toluene. J. Biol. Chem. **281:**11981–11991.
20. **Duetz, W. A., J. B. van Beilen, and B. Witholt.** 2001. Using proteins in their natural environment: potential and limitations of microbial whole-cell hydroxylations in applied biocatalysis. Curr. Opin. Biotechnol. **12:**419–425.
21. **Gage, D. J., and F. C. Neidhardt.** 1993. Adaptation of *Escherichia coli* to the uncoupler of oxidative phosphorylation 2,4-dinitrophenol. J. Bacteriol. **175:**7105–7108.
22. **Garrigues, C., P. Loubiere, N. D. Lindley, and M. Cocaign-Bousquet.** 1997. Control of the shift from homolactic acid to mixed-acid fermentation in *Lactococcus lactis*: predominant role of the NADH/NAD^+ ratio. J. Bacteriol. **179:**5282–5287.
23. **Gross, R., K. Lang, K. Buhler, and A. Schmid.** 2010. Characterization of a

biofilm membrane reactor and its prospects for fine chemical synthesis. Biotechnol. Bioeng. **105:**705–717.
24. **Hartig, C., N. Loffhagen, and H. Harms.** 2005. Formation of trans fatty acids is not involved in growth-linked membrane adaptation of *Pseudomonas putida*. Appl. Environ. Microbiol. **71:**1915–1922.
25. **Heyland, J., J. A. Fu, and L. M. Blank.** 2009. Correlation between TCA cycle flux and glucose uptake rate during respiro-fermentative growth of *Saccharomyces cerevisiae*. Microbiology **155:**3827–3837.
26. **Hou, J., N. F. Lages, M. Oldiges, and G. N. Vemuri.** 2009. Metabolic impact of redox cofactor perturbations in *Saccharomyces cerevisiae*. Metab. Eng. **11:**253–261.
27. **Igamberdiev, A. U., and L. A. Kleczkowski.** 2009. Metabolic systems maintain stable non-equilibrium via thermodynamic buffering. Bioessays **31:**1091–1099.
28. **Isken, S., A. Derks, P. F. Wolffs, and J. A. de Bont.** 1999. Effect of organic solvents on the yield of solvent-tolerant *Pseudomonas putida* S12. Appl. Environ. Microbiol. **65:**2631–2635.
29. **Koebmann, B. J., H. V. Westerhoff, J. L. Snoep, D. Nilsson, and P. R. Jensen.** 2002. The glycolytic flux in *Escherichia coli* is controlled by the demand for ATP. J. Bacteriol. **184:**3909–3916.
30. **Koebmann, B. J., et al.** 2002. The extent to which ATP demand controls the glycolytic flux depends strongly on the organism and conditions for growth. Mol. Biol. Rep. **29:**41–45.
31. **Leif, H., V. D. Sled, T. Ohnishi, H. Weiss, and T. Friedrich.** 1995. Isolation and characterization of the proton translocating NADH ubiquinone oxidoreductase from *Escherichia coli*. Eur. J. Biochem. **230:**538–548.
32. **León, R., P. Fernandes, H. M. Pinheiro, and J. M. S. Cabral.** 1998. Whole-cell biocatalysis in organic media. Enzyme Microb. Technol. **23:**483–500.
33. **Leonardo, M. R., Y. Dailly, and D. P. Clark.** 1996. Role of NAD in regulating the *adhE* gene of *Escherichia coli*. J. Bacteriol. **178:**6013–6018.
34. **Nanchen, A., A. Schicker, and U. Sauer.** 2006. Nonlinear dependency of intracellular fluxes on growth rate in miniaturized continuous cultures of *Escherichia coli*. Appl. Environ. Microbiol. **72:**1164–1172.
35. **Neves, A. R., et al.** 2002. Is the glycolytic flux in *Lactococcus lactis* primarily controlled by the redox charge? Kinetics of NAD^+ and NADH pools determined *in vivo* by ^{13}C NMR. J. Biol. Chem. **277:**28088–28098.
36. **Nikolova, P., and O. P. Ward.** 1993. Whole cell biocatalysis in nonconventional media. J. Ind. Microbiol. **12:**76–86.
37. **Otto, K., K. Hofstetter, M. Rothlisberger, B. Witholt, and A. Schmid.** 2004. Biochemical characterization of StyAB from *Pseudomonas* sp. strain VLB120 as a two-component flavin-diffusible monooxygenase. J. Bacteriol. **186:**5292–5302.
38. **Panke, S., A. Meyer, C. M. Huber, B. Witholt, and M. G. Wubbolts.** 1999. An alkane-responsive expression system for the production of fine chemicals. Appl. Environ. Microbiol. **65:**2324–2332.
39. **Panke, S., B. Witholt, A. Schmid, and M. G. Wubbolts.** 1998. Towards a biocatalyst for (*S*)-styrene oxide production: characterization of the styrene degradation pathway of *Pseudomonas* sp. strain VLB120. Appl. Environ. Microbiol. **64:**2032–2043.
40. **Park, J. B., B. Buhler, S. Panke, B. Witholt, and A. Schmid.** 2007. Carbon metabolism and product inhibition determine the epoxidation efficiency of solvent-tolerant *Pseudomonas* sp. strain VLB120ΔC. Biotechnol. Bioeng. **98:**1219–1229.
41. **Pirt, S. J.** 1965. Maintenance energy of bacteria in growing cultures. Proc. R Soc. Lond. B Biol. Sci. **163:**224–231.
42. **Sambrook, J., and D. W. Russell.** 2001. Molecular cloning: a laboratory manual, 3rd ed. Cold Spring Harbor Laboratory Press, Cold Spring Harbor, NY.
43. **Sauer, M., D. Porro, D. Mattanovich, and P. Branduardi.** 2008. Microbial production of organic acids: expanding the markets. Trends Biotechnol. **26:**100–108.
44. **Schaaff, I., J. Heinisch, and F. K. Zimmermann.** 1989. Overproduction of glycolytic enzymes in yeast. Yeast **5:**285–290.
45. **Smits, T. H. M., M. A. Seeger, B. Witholt, and J. B. van Beilen.** 2001. New alkane-responsive expression vectors for *Escherichia coli* and *Pseudomonas*. Plasmid **46:**16–24.
46. **Stephanopoulos, G., A. A. Aristidou, and J. Nielsen.** 1998. Metabolic engineering: principles and methodologies. Academic Press, San Diego, CA.
47. **Tomlin, K. L., S. R. D. Clark, and H. Ceri.** 2004. Green and red fluorescent protein vectors for use in biofilm studies of the intrinsically resistant *Burkholderia cepacia* complex. J. Microbiol. Methods **57:**95–106.
48. **van Beilen, J. B., W. A. Duetz, A. Schmid, and B. Witholt.** 2003. Practical issues in the application of oxygenases. Trends Biotechnol. **21:**170–177.
49. **Vemuri, G. N., M. A. Eiteman, and E. Altman.** 2006. Increased recombinant protein production in *Escherichia coli* strains with overexpressed water-forming NADH oxidase and a deleted ArcA regulatory protein. Biotechnol. Bioeng. **94:**538–542.
50. **Vemuri, G. N., M. A. Eiteman, J. E. McEwen, L. Olsson, and J. Nielsen.** 2007. Increasing NADH oxidation reduces overflow metabolism in *Saccharomyces cerevisiae*. Proc. Natl. Acad. Sci. U. S. A. **104:**2402–2407.
51. **Wohlgemuth, R.** 2009. The locks and keys to industrial biotechnology. New Biotechnol. **25:**204–213.
52. **Yu, J., et al.** 2001. Characterization of the *Streptococcus pneumoniae* NADH oxidase that is required for infection. Microbiology **147:**431–438.
53. **Zamboni, N., E. Fischer, and U. Sauer.** 2005. FiatFlux—a software for metabolic flux analysis from ^{13}C-glucose experiments. BMC Bioinformatics **6:**209.